

# Tropospheric ozone profiles by DIAL at Maïdo Observatory (Reunion Island): system description, instrumental performance, and result comparison with ozone external data set

Valentin Dufлот<sup>1,2</sup>, Jean-Luc Baray<sup>3</sup>, Guillaume Payen<sup>2</sup>, Nicolas Marquestaut<sup>2</sup>, Françoise Posny<sup>1</sup>, Jean-Marc Metzger<sup>2</sup>, Bavo Langerock<sup>4</sup>, Corinne Vigouroux<sup>4</sup>, Juliette Hadji-Lazarou<sup>5</sup>, Thierry Portafaix<sup>1</sup>, Martine De Mazière<sup>4</sup>, Pierre-François Coheur<sup>6</sup>, Cathy Clerbaux<sup>5,6</sup>, and Jean-Pierre Cammas<sup>1,2</sup>

<sup>1</sup>Laboratoire de l'Atmosphère et des Cyclones (LACy), UMR8105, Saint-Denis de La Réunion, France

<sup>2</sup>Observatoire des Sciences de l'Univers de La Réunion (OSUR), UMS3365, Saint-Denis de la Réunion, France

<sup>3</sup>Laboratoire de Météorologie Physique (LaMP), UMR6016, Observatoire de Physique du Globe de Clermont-Ferrand, CNRS - Université Blaise Pascal, Clermont-Ferrand, France

<sup>4</sup>Royal Belgian Institute for Space Aeronomy (BIRA-IASB), 3, Av. Circulaire, 1180, Brussels, Belgium

<sup>5</sup>LATMOS/IPSL, UPMC Univ. Paris 06 Sorbonne Universités, UVSQ, CNRS, Paris, France

<sup>6</sup>Spectroscopie de l'Atmosphère, Service de Chimie Quantique et Photophysique, Université Libre de Bruxelles (ULB), Brussels, Belgium

*Correspondence to:* Valentin Dufлот (valentin.dufлот@univ-reunion.fr)

**Abstract.** Recognizing the importance of ozone ( $O_3$ ) in the troposphere and lower stratosphere in the tropics, a DIAL (Differential Absorption Lidar) tropospheric  $O_3$  lidar system (LIO3T<sub>UR</sub>) was developed and installed at the Université de la Réunion campus site (close to the sea) in Reunion Island (southern tropics) in 1998. From 1998 to 2010, it acquired 427  $O_3$  profiles from the low to the upper troposphere and has been central to several studies. In 2012, the system was moved up to the new Maïdo Observatory facility (2160m above mean sea level - amsl) where it started operation in February 2013. The current system (LIO3T) configuration generates a 266nm beam obtained with the fourth harmonic of a Nd:YAG laser sent into a Raman cell filled up with deuterium (using helium as buffer gas) generating the 289 and 316nm beams enabling the use of the DIAL method for  $O_3$  profile measurements. Optimal range for the actual system is 6-19km amsl, depending on the instrumental and atmospheric conditions; for a 1-hour integration time, vertical resolution varies from 0.7km at 6km amsl to 1.3km at 19km amsl, and mean uncertainty within the 6-19km range is between 6 and 13%. Comparisons with 8 electrochemical concentration cell (ECC) sondes simultaneously launched from the Maïdo Observatory show a good agreement between datasets with a 6.8% mean absolute relative difference ( $D$ ) between 6 and 17km amsl (LIO3T lower than ECC); comparisons with 37 ECC sondes launched from the nearby Gillot site during day time in a  $\pm 24$ -hour window around lidar shooting result in a 9.4%  $D$  between 6 and 19km amsl (LIO3T lower than ECC); comparisons with 11 ground-based Network for Detection of Atmosphere Composition Change (NDACC) Fourier Transform Infrared (FTIR) spectrometer measurements acquired during day time in a  $\pm 24$ -hour window around lidar shooting show a good agreement between datasets with a  $D$  of 11.8% for the 8.5-16km partial column (LIO3T higher than FTIR); and comparisons with 39 simultaneous Infrared Atmospheric Sounding Interferometer (IASI) observations over Reunion Island show a good agreement between datasets with a  $D$  of 11.3% for the 6-16km partial column (LIO3T higher than IASI). ECC, LIO3T<sub>UR</sub> and LIO3T  $O_3$  monthly climatologies all exhibit the same

range of values and patterns. In particular, the southern hemisphere biomass burning seasonal enhancement, the ozonopause altitude decrease in late austral winter-spring, as well as the signature of deep convection bringing boundary layer-O<sub>3</sub> poor air masses up to the mid-upper troposphere in late austral summer, are clearly visible on all datasets.

## 1 Introduction

5 Because of its interaction with solar and terrestrial radiation, ozone (O<sub>3</sub>) is an important contributor to Earth's radiative balance, and any changes in its atmospheric distribution contribute to the radiative forcing of climate change (Lacis et al., 1990). O<sub>3</sub> is also an important pollutant, and impacts the oxidative capacity of the atmosphere (Martin et al., 2003). In the troposphere, the O<sub>3</sub> budget is influenced by transport from the stratosphere, by in situ photochemical production associated with O<sub>3</sub> precursors emitted by anthropogenic activity, biomass burning, lightning and by surface deposition (Stevenson et al., 2006).

10 Reunion Island is a tropical island located in the south-western part of the Indian Ocean at 20.8°S and 55.5°E. It is seasonally impacted by biomass burning plumes transported from Southern Africa, South America and South-East Asia which can significantly affect the free tropospheric concentrations of O<sub>3</sub> and other pollutants like CO (Edwards et al., 2006 ; Dufлот et al., 2010). Moreover, it is affected by stratospheric intrusions associated with the dynamical influence of the subtropical jet stream (Baray et al., 1998; Clain et al., 2010) and the tropical cyclone deep convection (Leclair de Bellevue et al., 2006).

15 The barrier effect and dynamical exchanges between the tropical reservoir and midlatitudes, and vertically between the troposphere and the stratosphere, affect the O<sub>3</sub> balance and distribution in both the troposphere and stratosphere, and are then of great interest to document climate change. Tropospheric O<sub>3</sub> measurements are performed routinely in Reunion Island by O<sub>3</sub> sondes at the Gillot site (cf. Figure 1 and Table 1) since 1992 (in the framework of the Network for the Detection of Atmospheric Composition Change - NDACC since 1996 and of Southern Hemisphere ADDitionaln OZone sondes - SHADOZ  
20 network since 1998), and by lidar at the Université de la Réunion campus site (cf. Figure 1 and Table 1) since 1998 (Baray et al., 1999, 2006).

To improve the ability of the ground-based remote sensing instruments to probe the upper-troposphere/lower-stratosphere (UT/LS) region, a high atmospheric facility was built in 2012 at the summit of the Maïdo mount (cf. Figure 1 and Table 1), and most of the instruments previously installed close to the coast at the Université de la Réunion campus site were moved up to  
25 this new facility along the year 2012 (Baray et al., 2013). Being inside the boundary layer during the day and most of the time inside the free troposphere during the night (except during the warm and rainy season), the Maïdo Observatory is dedicated to the investigation of the boundary layer composition and processes (especially in the framework of the Global Atmospheric Watch network - GAW), as well as to the study of the low-middle atmosphere (especially in the framework of the NDACC). Four lidar systems are permanently deployed and routinely operated at the Maïdo Observatory:

- 30
- a Doppler wind lidar dedicated to the study of the middle atmosphere dynamics (Khaykin et al., 2015),
  - the LIO3S, a lidar dedicated to stratospheric O<sub>3</sub> measurements (Portafaix et al., 2003; Portafaix et al., 2015),

- the LI1200, a lidar dedicated to tropospheric water vapor (Hoareau et al., 2012; Dionisi et al., 2015; V er emes et al., 2017) and stratospheric-mesospheric temperature measurements (Morel et al., 2002; Keckhut et al., 2004, 2015; Sivakumar et al., 2011a),

- and the LIO3T lidar (Baray et al., 1999, 2006; Clain et al., 2009, 2010; V er emes et al., 2016) dedicated to the observation of tropospheric O<sub>3</sub> (as well as aerosols from the free troposphere up to the lower stratosphere).

It is noteworthy that the LIO3T system was very recently affiliated in the NDACC for O<sub>3</sub> measurements ; this paper aims to provide a technical reference socle for further use of the O<sub>3</sub> data provided by the LIO3T system: we first present the data processing, we then give a brief historical review of the tropospheric O<sub>3</sub> lidar system when installed at the Universit e de la R eunion campus site (1998-2010) together with a description of the current LIO3T system installed at the Ma ido Observatory.

We show comparisons between the LIO3T O<sub>3</sub> measurements and O<sub>3</sub> external dataset. We finally present an overview of the lidar tropospheric O<sub>3</sub> profiles database.

In the following, the system will be referred as "LIO3T<sub>UR</sub>" when it was installed at the Universit e de la R eunion, and the current system (installed at the Ma ido Observatory) will be referred as "LIO3T".

## 2 Data processing

The program used to calculate the O<sub>3</sub> profile, uncertainties and resolution is adapted from the stratospheric O<sub>3</sub> program "DIAL", which has been described and inter-compared by Godin et al. (1999) and is currently used for the stratospheric DIAL O<sub>3</sub> retrievals at Reunion (NDACC affiliated).

### 2.1 Lidar equation

The lidar DIAL (Differential Absorption Lidar) technique (Hinkley, 1976) relies on the difference between two backscattered lidar signals at two different wavelengths, one where O<sub>3</sub> is strongly absorbed (ON, here: 289nm) and the other one where O<sub>3</sub> absorption is weaker (OFF, here: 316nm). The O<sub>3</sub> number density  $n_{O_3}(z)$  at altitude  $z$  (in molec/cm<sup>3</sup>) is retrieved from the Rayleigh lidar signals according to the following equation (Harris at al., 1998):

$$n_{O_3}(z) = \frac{-1}{2\Delta\sigma_{O_3}(z)} \frac{d}{dz} \left[ \ln \left( \frac{P(\lambda_{ON}, z) - B(\lambda_{ON}, z)}{P(\lambda_{OFF}, z) - B(\lambda_{OFF}, z)} \right) \right] + \delta n_{O_3}(z) \quad (1)$$

where  $\Delta\sigma_{O_3}(z) = \sigma_{O_3}(\lambda_{ON}, z) - \sigma_{O_3}(\lambda_{OFF}, z)$  is the differential O<sub>3</sub> absorption cross-section,  $P(\lambda_i, z)$  is the number of detected photons,  $B(\lambda_i, z)$  is the background noise and detector noise, and  $\delta n_{O_3}(z)$  is a correction term corresponding to the absorption by other constituents of the atmosphere, expressed as follows:

$$\delta n_{O_3}(z) = \frac{1}{\Delta\sigma_{O_3}(z)} \left[ \frac{1}{2} \frac{d}{dz} \left[ \ln \left( \frac{\beta(\lambda_{ON}, z)}{\beta(\lambda_{OFF}, z)} \right) \right] - \Delta\sigma_{atm}(z)n_{atm} - \sum_{ig} \Delta\sigma_{ig}(z)n_{ig}(z) \right] \quad (2)$$

where  $\beta(\lambda_i, z)$  is the coefficient of extinction of the molecules and particles,  $\Delta\sigma_{atm}(z)$  and  $n_{atm}$  the differential cross-section and the density of the atmosphere, respectively, and  $\Delta\sigma_{ig}(z)$  and  $n_{ig}(z)$  the differential cross-section and the number density of interfering gas  $ig$ , respectively. According to Leblanc et al. (2016b), the interfering gases to consider in practice are NO<sub>2</sub>, SO<sub>2</sub>, and O<sub>2</sub>. NO<sub>2</sub> and SO<sub>2</sub> are negligible in most cases of tropospheric O<sub>3</sub> retrieval, except in heavy volcanic aerosols loading conditions. The absorption by O<sub>2</sub> should be considered if any of the detection wavelength is shorter than 294nm (which is the case here as we use the 289nm wavelength). However, in our case, we do not take into account in our retrieval any interfering gases for the time being. It is part of our future plans to include them in the "DIAL" code. The background light, the saturation of the detector and the noise from detectors must be added to this equation (2).

## 2.2 Saturation, correction and vertical resolution

The saturation is defined as the phenomenon in which the amount of output signal is no longer proportional to the incident light intensity. It is a non-linear phenomenon, depending on the dead time of the detector. In the LIO3T case, due to the detector sensitivity and the geometry of the instrument, we found that saturation occurs only below 7km. To correct it, we apply the scheme described in Pelon (1985, Annex 2):

$$N_c = 1 + \left[ \left( 1 - \frac{\tau}{\delta t} \right) N_r - 1 \right] e^{-\frac{\tau}{\delta t} N_r} \quad (3)$$

with  $N_c$  the number of photons counted,  $N_r$  the number of photons received,  $\tau$  the dead time of the detector and  $\delta t$  the integration time.

The vertical resolution is directly linked to the filtering of the lidar signal. For LIO3T<sub>UR</sub>, the signal was filtered using a Taylor derivative filter together with a polynomial low pass filter of order 2, and for LIO3T, we filter the signal with the Savitzky-Golay derivative filter of order 2, also called least-squares smoothing filter (Savitzky and Golay, 1964). To take into account the decreasing signal-to-noise ratio with altitude, the number of points of the used filters (for both LIO3T<sub>UR</sub> and LIO3T) increases with altitude (and, consequently, the vertical resolution decreases with altitude, cf. Section 3.2 and Figure 3). To calculate the resulting vertical resolution, the frequency approach detailed in Leblanc et al. (2016a) is used.

## 2.3 Uncertainty

Uncertainties calculation for DIAL O<sub>3</sub> retrievals are described in Leblanc et al. (2016b). The most significant sources of uncertainties are found to be the detection noise, the O<sub>3</sub> cross section uncertainties and the background noise.

Using our acquisition card in photon-counting mode, we calculate the detection noise by assuming that the signal's standard deviation is equal to that which is expected for a Poisson statistical distribution of detected photons. The corresponding uncertainty is thus estimated directly from the signal intensity (Leblanc et al., 2016b - equations (28) and (29)).

Molina and Molina (1986) and Bass and Paur (1984) O<sub>3</sub> cross sections were used for O<sub>3</sub> profile retrieval for LIO3T<sub>UR</sub> and LIO3T, respectively, both with an uncertainty equal to 5%.

The background noise includes the background light, which is altitude-independent, and the detector noise - dark noise and induced signals -, which are altitude-dependent. We extract the background noise from the lidar signal by fitting the uppermost part of the lidar signal using a linear or polynomial regression function and by subtracting the result from the signal.

To take into account the propagation of these errors in the lidar equation, and assuming that all uncertainties are independent, we follow the approach detailed by Leblanc et al. (2016b - equation 4 with no covariance term).

### 3 Instrumental description and performances

#### 3.1 Historical context and main instrumental features

A Rayleigh-Mie lidar was first installed at the Université de la Réunion campus site in 1993 to monitor stratospheric and mesospheric aerosols in the southern tropics. From 1993 to 1998, the lidar system evolved both in terms of emission and reception (Nd:YAG laser replacement, mosaic telescopes addition, polarization channels installation, infrared channel reception set up) to improve aerosols detection and characterization, and to allow stratospheric-mesospheric temperature measurement.

In 1998, an extension was installed to the existing system to perform O<sub>3</sub> measurements in the free troposphere, including the upper troposphere. Baray et al. (1999) give a complete description of the LIO3T<sub>UR</sub> and provide justifications of the technical choices that were made at this time. Note that the first "home made" acquisition chain was changed for a LICEL one in 2007, but this change did not cause significant differences in the profiles acquired.

Late 2012, the Maïdo Observatory new facility was complete and the fixed lidar systems were moved from the Université de la Réunion campus site and installed in the Observatory. Since temperature measurements are now performed with the LI1200 system - also dedicated to water vapor measurement (Dionisi et al., 2015; Vérèmes et al., 2017) - the previous LIO3T<sub>UR</sub> was modified into a system dedicated to the measurement of tropospheric O<sub>3</sub> (and aerosols): the "LIO3T".

Figure 2 sketches the experimental schematic of the O<sub>3</sub> DIAL part of the LIO3T and gives its main technical characteristics. The LIO3T mainly relies on the LIO3T<sub>UR</sub> design (Baray et al., 1999). We use the same approach to generate a 266nm beam going through a deuterium filled Raman cell (using helium as buffer gas) shifting the incoming frequency to 289 and 316nm signals, and the backscattered photons are collected by the same 4x500mm-telescope mosaic focusing on 1.5mm diameter optical fibers. Hamamatsu R9880-110 and R7400P-03 photomultiplier tubes are used, for 289 and 316 nm channels, respectively. Further details on the LIO3T features can be found in Baray et al. (2013).

For information, the detection and characterization of the tropospheric aerosols by the LIO3T is currently performed using the emitted 532nm "residual" beam, a 200mm telescope for reception of the elastic signal, and a polarization detection system. This aerosols detection wing of the LIO3T will be the subject of dedicated studies.

#### 3.2 Performances

The LIO3T<sub>UR</sub> was only operated at night to increase the signal-to-noise ratio (Kovalev and Eichinger, 2004). Due to the overlap factor (the height where the telescope's field-of-view and laser beam overlap completely, and above which it remains constant)

and detection limit, the LIO3T<sub>UR</sub> optimal range was 3.5-17km above mean sea level (amsl) (Baray et al., 1999). Note that in the following all altitudes will be given amsl. Figures 3 and 4 give the mean vertical resolution and uncertainty profiles for LIO3T<sub>UR</sub> over the 13 years of operation. The temporal resolution (or integration time) depended on the atmospheric conditions (i.e. the cloud free sky duration) and varied roughly between 40 minutes and 3 hours. Vertical resolution varies from 0.1km at 3km to 1.8km at 17km. The mean uncertainty varies from  $\approx 6\%$  ( $\approx 3.8 \times 10^{10}$  molec/cm<sup>3</sup>) at 3km to  $\approx 15\%$  ( $\approx 7 \times 10^{10}$  molec/cm<sup>3</sup>) at 16km, and increases up to  $60\%$  ( $\approx 3.5 \times 10^{11}$  molec/cm<sup>3</sup>) at 17km (not shown) where the detection noise dominates.

The altitude of the Maïdo Observatory being 2160m, the transfer of the tropospheric O<sub>3</sub> DIAL system from the University (80m) to this location increases the upper limit of the profile probed, but also increases the lower limit: the optimal range is now 6-19km. The free troposphere, the tropical tropopause layer (TTL) and lower stratosphere are thus covered by the current system. It is worth mentioning, however, that depending on experimental conditions (lidar alignment, stability of emitted power at the transmitted wavelength, atmospheric conditions, etc.), the validity domain can vary from one day to another.

Similarly to the LIO3T<sub>UR</sub>, the LIO3T is only operated at night to increase the signal-to-noise ratio, and twice a week in routine conditions (i.e. out of campaigns). We use three main integration times: 20 minutes for night time series, 1 hour for comparison with collocated ECC soundings (1 hour is roughly the time for the balloon to travel the troposphere), and  $\approx 3$  hours (between  $\approx 2$  and  $\approx 4$  hours, depending on the clear sky time duration) for "full night" profiles. Figure 3 also shows the vertical resolution resulting from each of these integration times for LIO3T. For the 20-minutes integration time, the resulting resolutions are 0.9 and 1.6 km at 6 and 19 km, respectively; for the 1-hour integration time, they are 0.7 and 1.3 km at 6 and 19 km, respectively; and for the 3-hour integration time, 0.3 and 1.2 km. The difference between the LIO3T<sub>UR</sub> and LIO3T vertical resolutions results from the use of different filters and numbers of points for the signal filtering (cf. Section 2.2).

Figure 4 also shows the mean uncertainties for LIO3T for the three main integration times in % (left panel) and molec/cm<sup>3</sup> (right panel). For the three integration times, mean uncertainty varies between  $\approx 7\%$  ( $\approx 6 \times 10^{10}$  molec/cm<sup>3</sup>) at 6km and  $\approx 5\%$  ( $\approx 5.5-8 \times 10^{10}$  molec/cm<sup>3</sup>) at 19km with a peak at  $\approx 10\%$  ( $\approx 5 \times 10^{10}$  molec/cm<sup>3</sup>),  $\approx 12\%$  ( $\approx 6 \times 10^{10}$  molec/cm<sup>3</sup>) and  $\approx 15\%$  ( $\approx 7.5 \times 10^{10}$  molec/cm<sup>3</sup>) at 16km for the >1 hour, 1 hour and 20 minutes integration time, respectively. These figures are in agreement with the recently published work of Leblanc et al. (2016b) showing uncertainty profiles for a 2h DIAL tropospheric O<sub>3</sub> measurement between 7 and 11%. One can notice that, above 16km, the LIO3T<sub>UR</sub> uncertainty increases and is greater than the LIO3T one; oppositely, the LIO3T uncertainty decreases (in %) between 16 and 19km. This can be explained by the fact that the LIO3T<sub>UR</sub> reaches its detection limit between  $\approx 16$ km and  $\approx 17$ km (where the detection noise dominates), while for the LIO3T the increase of the detection noise is balanced by the increase of the O<sub>3</sub> abundance when entering the stratosphere.

The main benefit from the instrument altitude change from 80m to 2160m is to enable it to document the UT/LS region with relevant vertical and time resolutions together with a reasonable uncertainty (1.5km, 20min and 10%, respectively, at 18km).

## 4 Comparisons of LIO3T measurements with O<sub>3</sub> external dataset

The goal of this section is to validate the LIO3T O<sub>3</sub> measurements by comparing them to O<sub>3</sub> external dataset. Four types of correlative data are used here: 8 collocated ECC soundings (i.e. launched from the Maïdo Observatory during a lidar shooting), 37 routine NDACC/SHADOZ ECC soundings performed during daytime at the Gillot site (cf. Figure 1 and Table 1), and 5 Fourier Transform InfraRed spectrometer (FTIR) tropospheric partial columns measurements from both daytime ground-based (12 comparison pairs) and nighttime Infrared Atmospheric Sounding Interferometer (IASI) (39 comparison pairs) data.

In the following, we compare  $N$  LIO3T O<sub>3</sub> measurements  $M_{LIO3T}$  with  $N$  correlative data  $M_{CD}$  by calculating the mean absolute relative difference between datasets  $D$  (in %) defined as:

$$D = \frac{1}{N} \sum_{n=1}^N |r_n| \quad (4)$$

10 with  $r_n$  the relative difference (in %) between two observations  $M_{LIO3T_n}$  and  $M_{CD_n}$  defined as:

$$r_n = 100 * \frac{M_{LIO3T_n} - M_{CD_n}}{\frac{M_{LIO3T_n} + M_{CD_n}}{2}} \quad (5)$$

### 4.1 Comparison with ECC

ECC sondes measure the oxidation of a potassium iodine (KI) solution by O<sub>3</sub> (Komhyr et al., 1995). Their precision is 5-10% throughout the troposphere and TTL (Smit et al., 2007) and they are commonly used for the validation of ground-based and 15 space-borne O<sub>3</sub> observations. Here below, we compare LIO3T O<sub>3</sub> profiles with both collocated Maïdo ECC soundings and Gillot SHADOZ/NDACC routine daytime ECC soundings. All these ECC profiles are generated following the "Guidelines for homogenization of ozonesonde data" (Smit et al., 2012). The Gillot SHADOZ/NDACC reprocessed ECC dataset was recently presented by Posny et al. (2016), Smit et al. (2016) and Witte et al. (2017) and is used in this article. Moreover, similar reprocessing was applied on the ECC soundings performed at the Maïdo Observatory. From August 2007 to December 2016, 20 ECC soundings were performed at Reunion Island using the ENSCI/0.5% full buffer solution, instead of the standard half buffer. This specificity of the Reunion Island ECC soundings is not taken into account in the SHADOZ/NDACC reprocessed ECC dataset yet. Following the work of Johnson et al. (2002, 2016) intercomparing various KI and buffer solutions, we found that this ENSCI/0.5% full buffer solution tends to overestimate the amount of O<sub>3</sub> by 1.7% in average in the troposphere. Consequently, an adapted correction was applied on the ECC profiles acquired during this period.

25 Figure 5 shows the comparison between LIO3T and 8 ECC soundings collocated in time and space: two were performed in June 2013, four in May 2015 and two in July 2015. Note that these last six were part of the Maïdo ObservatoRy Gaz and Aerosols Ndacc Experiment (MORGANE) campaign that took place in May-July 2015 (Portafaix et al., 2015; Dufлот et al., 2016a; Posny et al., 2016; Vèrèmes et al., 2017). The integration time for the LIO3T profiles used here is 1h (starting at the ECC sonde launch time) and corresponds roughly to the time for the balloon to travel the troposphere. Note that the

”discontinuities” in the mean profiles shown on Figure 8 are caused by the varying valid ranges in the LIO3T profiles (cf. Table 2), and note that no profile goes above 17km for these eight comparisons. In particular, the valid range in May and July 2015 (during the MORGANE campaign) is bounded up at 17km by the volcanic aerosol loading coming from the Calbuco volcano (Chile, 41.32°S, 72.62°W), which erupted late April 2015 and whose volcanic plume reached the TTL above Reunion Island on the 6th May 2015 before slowly vanishing near the end of July 2015 (Bègue et al., 2017). This aerosol enhancement is clearly visible on the 355nm channels of the stratospheric O<sub>3</sub> and LI1200 lidars, and on the 532nm channel of the LIO3T (not shown), and back trajectories together with CALIOP observations (on board CALIPSO - not shown) show that the detected plume comes from the Calbuco volcano (Bègue et al., 2017). Consequently, although we do not have any information on the corresponding aerosol and SO<sub>2</sub> amount, we consider as a wise assumption that, in the layer where this volcanic plume lies (i.e. between 17 and 22km), the SO<sub>2</sub> and aerosols loading is too strong to allow a correct O<sub>3</sub> retrieval (Ancellet et al., 1987; McGee et al., 1993).

One can see on Figure 5 that there is an overall agreement between LIO3T and the ECC considering the lidar uncertainty and ECC precision (right panel).  $D$  is 6.8% for the whole probed column (LIO3T lower than ECC). This value agrees with the ones recently reported for single or multiple ECC-lidar comparisons (between 6 and 20% reported by Uchino et al., 2014; 20% reported by Sullivan et al., 2015; 8% reported by Gaudel et al., 2015).

Figure 6 shows the comparison between the SHADOZ/NDACC Gillot routine ECC soundings and LIO3T profiles. As the first ones are performed during daytime (usually around 15:00:00 LT) and the last ones during night time (between 19:00:00 and 01:00:00 LT), ECC soundings are taken into consideration when performed one day before or after a LIO3T profile acquisition; we find 37 pairs for comparison over the years 2013-2015. The LIO3T profiles used here are ”full night” profiles. Once again, note that the ”discontinuities” in the mean profiles shown on Figure 6 are caused by the varying valid ranges in the LIO3T profiles (and one can see that only one profile is above 18km). Despite the fact that the instruments were neither collocated in time nor space (the ECC launch site - Gillot - is 26km away from the Maïdo Observatory (cf. Table 1) and balloons are advected by the wind), one can see that there is an overall good agreement between measurements considering the lidar uncertainty and ECC precision, with a mean  $D$  equal to 9.4% over the entire 6-19km column (LIO3T lower than ECC).

## 4.2 Comparison with ground-based and space-borne FTIRs

In this section we compare the LIO3T profiles with collocated partial column measurements performed by two FTIRs: the Bruker 125HR installed at the Maïdo Observatory since 2013, and IASI on board the MetOp-A satellite.

### 4.2.1 Comparison with NDACC ground-based FTIR measurements

A Bruker 125HR FTIR spectrometer started operating at the Maïdo Observatory in March 2013 with a primary dedication to NDACC measurements (Zhou et al., 2016). This NDACC ground-based FTIR observes the absorption of the direct solar radiation with high spectral resolution ( $0.0035\text{-}0.0110\text{ cm}^{-1}$ ) and uses the pressure broadening effect of absorption lines to retrieve volume mixing ratio (vmr) low vertical resolution profiles of target gases. The FTIR O<sub>3</sub> measurements show a good sensitivity from the ground up to about 45 km. Within this vertical range, about 4 vertical layers can be distinguished, i.e.



the vertical resolution varies from 8 to 15 km (Vigouroux et al., 2015). In this study, the FTIR retrievals are based on an optimal estimation method (Rodgers, 2000), carried out with the SFIT4 algorithm (<https://wiki.ucar.edu/display/sfit4>), which is an open source code, jointly developed at the NASA Langley Research Center, the National Center for Atmospheric Research (NCAR), the National Institute of Water and Atmosphere Research (NIWA) and University of Bremen. HBr cell measurements are performed on a daily basis to verify the alignment of the instrument and to obtain the instrument line shape (ILS) using the LINEFIT14.5 program (Hase et al., 1999). The retrieval scheme is described in Vigouroux et al. (2015), and closely follows the recipe of the Jungfraujoch station (except for the ILS which is fixed from LINEFIT results at Maïdo): the retrieval microwindow is 1000-1005  $\text{cm}^{-1}$ , the a priori data comes from the WACCMv6 model and pressure and temperature a priori profiles were obtained from National Centers for Environmental Prediction. The a priori water profile is obtained from a dedicated pre-retrieval. Each  $\text{O}_3$  profile is retrieved with the signal to noise of the source spectrum. The total uncertainty on the  $\text{O}_3$  profile is dominated by the smoothing error (i.e. the poor vertical resolution of the profile), the temperature and the spectroscopic uncertainties. We use the following approach for comparison:

- i) FTIR performing observations during daytime, each LIO3T measurement is compared to all FTIR measurements within a 24-hour time window;
- ii) for each such a pair (114 pairs in total), the LIO3T profile is regridded consistently to the FTIR;
- iii) FTIR measurements are averaged within the 24-hour time window around a single LIO3T measurement for comparison;
- iv) at this stage we have a set of comparable pairs of measurements with various validity domain for LIO3T profiles; however, the method needs constant boundaries for the partial column used for comparison; we then choose the partial column shared by a sufficient number of LIO3T profiles to allow a reasonable comparison; the upper and lower limits of this partial column are called hereafter "valid range for comparison";
- v) the regridded LIO3T profile is smoothed with the FTIR averaging kernel matrix and a priori (see, e.g., Rodgers and Connor, 2003; Vigouroux et al., 2008); to allow for the smoothing, the LIO3T measured profiles are extended by the FTIR a priori outside the valid range for comparison. By smoothing the LIO3T profiles, we degrade them to the FTIR low vertical resolution, and we can get rid of the FTIR smoothing uncertainty in the uncertainty associated with the comparison;
- vi) finally, a partial column is calculated from this smoothed LIO3T profile in the valid range of comparison.

We find 12 comparison pairs over the studied period within the 8.5-16km valid range for comparison. In this 8.5-16km partial column, the ground-based NDACC FTIR has 1.1 degree of freedom (Rodgers, 2000) and a mean total uncertainty of 7.5%. Figure 7 shows the FTIR a priori profile and averaging kernels for this 8.5-16km partial column, both of them being used to smooth the LIO3T measurements to compare with the FTIR ones.

Figures 8 shows the comparison of the FTIR and LIO3T partial columns available over the 01/2013-01/2016 period. One can see that there is a good agreement between the datasets considering the uncertainties. We find a  $D$  of 11.8% between datasets (LIO3T higher than FTIR). Note that, due to the sparse comparison points, the southern hemisphere biomass burning season is not visible on this plot.

## 4.2.2 Comparison with IASI measurements

IASI is on board the MetOp-A satellite launched in a Sun-synchronous orbit around the Earth at the end of 2006. A second IASI was launched on board MetOp-B in September 2012 and the launch of the third one (MetOp-C) is planned for late 2018. In this comparison, IASI/MetOp-A data are used. IASI is a FTIR instrument that measures the thermal infrared radiation emitted by the Earth's surface and atmosphere in the  $645\text{-}2760\text{ cm}^{-1}$  spectral range with a spectral resolution of  $0.5\text{ cm}^{-1}$  apodized and a radiometric noise below  $0.2\text{K}$  between  $645$  and  $950\text{ cm}^{-1}$  at  $280\text{K}$  (Clerbaux et al., 2009).

IASI is an interesting instrument for our intercomparison effort as it provides global Earth coverage twice daily with overpass times at  $09:30:00$  and  $21:30:00$  mean local time and a nadir footprint on the ground of  $12\text{km}$ . IASI has significant sensitivity to tropospheric  $\text{O}_3$ . As LIO3T usually fires between  $19:00:00$  and  $01:00:00$  local times, we used here the IASI nighttime overpass measurements. The IASI data used in this study come from the FORLI- $\text{O}_3$  v20151001 scheme (Hurtmans et al., 2012; Boynard et al., 2016).

To compare measurements from both instruments, IASI retrievals are averaged over a  $1^\circ \times 1^\circ$  box around the Maïdo Observatory location. We then use the same approach as described in Section 4.2.1 (except points i) and iii)). We find 39 comparison pairs over the studied period within the  $6\text{-}16\text{km}$  valid range for comparison. In this  $6\text{-}16\text{km}$  partial column, IASI has 1.6 degree of freedom (Rodgers, 2000) and a mean total uncertainty equal to  $18.4\%$ . Figure 7 shows the mean IASI a priori profile and mean averaging kernels in the  $6\text{-}16\text{km}$  partial column for the 39 comparison pairs. In the following, LIO3T measurements are smoothed according to these characteristics of the IASI retrievals.

Figure 9 shows the comparison of the IASI and LIO3T partial columns time series. We obtain a good agreement between the datasets considering the uncertainties. We find a  $D$  of  $11.3\%$  between datasets (LIO3T higher than IASI). These results are in agreement with the  $5\text{-}15\%$   $\text{O}_3$  abundance difference of IASI in the troposphere compared to ECC soundings reported recently by Boynard et al. (2016). Note that, due to the sparse comparison points, the southern hemisphere biomass burning season is barely visible on this plot.

## 5 Dataset and climatologies

Figure 10 shows the monthly distribution of the number of  $\text{O}_3$  profiles acquired by the NDACC/SHADOZ ECC (Gillot, 1998-2015, 568 profiles), LIO3T<sub>UR</sub> (Université de la Réunion, 1998-2010, 427 profiles), and LIO3T (Maïdo Observatory, 2013-2015, 84 profiles). The low number of lidar profiles in the austral summer period (especially December-January) is explained by the high occurrence of cloudy skies. Especially, one can see that only one LIO3T profile is available for December (which ends up at  $10\text{km}$  due to a misalignment of the LIO3T). Lower limit of LIO3T profiles range from  $6$  to  $10\text{km}$ , and upper limit from  $12$  to  $19\text{km}$ . Most LIO3T profiles start at  $6\text{km}$  and end at  $17\text{-}18\text{km}$ .

Figure 11 shows the three resulting monthly tropospheric  $\text{O}_3$  climatologies, on which the following seasonal features can be observed:

- a clear increase of  $\text{O}_3$  abundance over the whole tropospheric column - especially between  $2$  and  $10\text{ km}$  - starting in June and ending in December with a maximum in October of  $\approx 10 \times 10^{11}\text{ molec/cm}^3$  on average between  $4$  and  $10\text{ km}$ ; this increase

is due to the influence of air masses coming from South America, Southern Africa and South-East Asia (Edwards et al., 2006; Dufлот et al., 2010) where the biomass burning season occurs every year during this period; O<sub>3</sub> abundance then presents a slow decay over the entire tropospheric column from January to May;

- the decrease of the ozonopause altitude from  $\approx 17$  km in December-July down to  $\approx 15$  km in August-November (Sivakumar et al., 2011b), which is likely a combination of the spring and summer maximum of occurrence of stratosphere-to-troposphere exchanges (STE) above Reunion Island (Clain et al., 2010) and of the winter time thermal effect on the troposphere thickness;
- the minimum of O<sub>3</sub> abundance in February between 10 and 16 km ( $\approx 3 \times 10^{11}$  molec/cm<sup>3</sup> on average), which is likely a signature of the austral summer deep convection bringing boundary layer-O<sub>3</sub> poor air masses up to the mid-upper troposphere.

In conclusion, the three datasets show a remarkable - and reassuring - agreement in terms of patterns and values.

- 10 Figure 12 shows the seasonal profiles derived from the LIO3T measurements. The southern hemisphere biomass burning season is still clearly visible in the September-October-November profile (SON), with an increase that covers the whole probed column, and also on the June-July-August (JJA) profile from 6 to 13 km.

## 6 Conclusions and future plans

- A DIAL tropospheric O<sub>3</sub> lidar was operating on the Université de la Réunion campus site from 1998 to 2010, providing 427  
15 O<sub>3</sub> profiles. In 2012, the system was moved up to the Maïdo Observatory and routine O<sub>3</sub> observations started in February 2013 by the LIO3T. From then until January 2016, 84 O<sub>3</sub> profiles were acquired and LIO3T operation is ongoing. These O<sub>3</sub> measurements were recently affiliated in the NDACC.

- The LIO3T observation scheme is based on the DIAL technique, which currently detects two wavelengths, 289 and 316 nm, with multiple receivers. The transmitted wavelengths are generated by focusing the output of a quadrupled Nd:YAG laser beam  
20 (266 nm) into a Raman cell, filled with high-pressure deuterium, using helium as buffer gas. With the knowledge of the O<sub>3</sub> absorption coefficient at these two wavelengths, the range-resolved number density can be derived.

Optimal range for the actual system is 6-19km, depending on the system performance and atmospheric conditions; for a 1-hour integration time, vertical resolution varies from 0.7 km at 6 km to 1.3 km at 19 km, and mean uncertainty over the 6-19km range is between  $\approx 6$  and  $\approx 13\%$ .

- 25 Comparisons with O<sub>3</sub> external dataset were performed showing a good agreement between datasets considering the uncertainties: we found a 6.8% *D* between LIO3T observations and 8 ECC sondes simultaneously launched from the Maïdo Observatory (LIO3T lower than ECC), 9.4% *D* between LIO3T observations and 37 ECC sondes launched from the Gillot site during day time in a  $\pm 24$ -hour window around lidar shooting (LIO3T lower than ECC), 11.8% *D* between LIO3T and 12 ground-based NDACC FTIR measurements acquired during day time in a  $\pm 24$ -hour window around lidar shooting in  
30 the 8.5-16 km partial column (LIO3T higher than FTIR), and 11.3% *D* between LIO3T and 39 simultaneous nighttime IASI observations over Reunion Island in the 6-16 km partial column (LIO3T higher than IASI).

ECC, LIO3T<sub>UR</sub> and LIO3T monthly climatologies all exhibit the same range of values and the same seasonal patterns:

- the O<sub>3</sub> abundance increase between 6 and 10 km in austral winter and spring due to the southern hemisphere biomass burning season;

- the ozonopause altitude decrease from  $\approx 17\text{km}$  to  $\approx 15\text{km}$  from late austral winter to early austral summer due to the winter time thermal effect on the troposphere thickness combined to the enhanced occurrence of STE in austral spring and summer;

- the O<sub>3</sub> abundance minimum between 10 and 16 km in late austral summer in the mid-upper troposphere due to deep convection uplifting O<sub>3</sub>-poor air masses from the boundary layer.

The move of this lidar from the Université de la Réunion campus site up to the Maïdo observatory allows it to document the UT/LS region and to follow stratospheric and tropospheric intrusions with relevant vertical and time resolutions together with a reasonable uncertainty (1.5km, 20min and 10%, respectively, at 18km). This tropospheric O<sub>3</sub> data set covering the tropical free troposphere and UT/LS of a sparsely documented region (South Western Indian Ocean) constitutes an extremely valuable resource for the validation of satellite tropospheric O<sub>3</sub> retrievals, analysis of the O<sub>3</sub> variability and sources, dynamics analysis of case studies, and for long term atmospheric monitoring.

Future plans for the LIO3T are to: (1) use the available 532nm residual beam to detect and study aerosols in the free troposphere, TTL and lower stratosphere. The use of the infrared signal (1064nm) to study aerosols is also planned; (2) implement NDACC recommendations in the data processing (O<sub>3</sub> cross sections, background and saturation corrections uncertainties propagation, interfering gases); (3) calculate uncertainties due to the presence of aerosols in the troposphere using an iterative aerosol assessment procedure, ideally using the 532nm backscattered signal.

*Acknowledgements.* The authors acknowledge the European Communities, the Région Réunion, CNRS, and Université de la Réunion for their support and contribution in the construction phase of the research infrastructure OPAR (Observatoire de Physique de l'Atmosphère de La Réunion). OPAR is presently funded by CNRS (INSU) and Université de La Réunion, and managed by OSU-R (Observatoire des Sciences de l'Univers de La Réunion, UMS 3365). The authors also gratefully acknowledge E. Golubic, P. Hernandez and L. Mottet who are deeply involved in the routine lidar observations at the Maïdo facility. J. Witte (NASA/GSFC) is acknowledged for the ECC data reprocessing. IASI is a joint mission of EUMETSAT and the Centre National d'Etudes Spatiales (CNES, France). The IASI L1C data are distributed in near real time by EUMETSAT through the EUMETCast system distribution. The authors acknowledge the Aeris data infrastructure for providing access to the IASI L1C data and L2 temperature data used in this study. This work was undertaken in the framework of the EUMETSAT O<sub>3</sub>M-SAF project (<http://o3msaf.fmi.fi>), the European Space Agency O<sub>3</sub> Climate Change Initiative (O<sub>3</sub>-CCI, [www.esa-ozone-cci.org](http://www.esa-ozone-cci.org)). The ULB French scientists are grateful to CNES and Centre National de la Recherche Scientifique (CNRS) for financial support. PFC is grateful to Belspo and ESA (Prodex IASIFlow project) for financial support. The colleagues from BIRA-IASB acknowledge the support from the Belgian Science Policy Office, as well as from ESA/PRODEX and the Copernicus programme (CAMS-VAL).

## References

- Ancellet, G., Mégie, G., Pelon, J., Capitini, R., and Renaut, D.: Lidar measurements of sulfur dioxide and ozone in the boundary layer during the 1983 Fos Berre Campaign, *Atmos. Environ.*, 21, 2215-2226, 1987.
- Baray, J.-L., Ancellet, G., Taupin, F. G., Bessafi, M., Baldy, S., and Keckhut, P.: Subtropical tropopause break as a possible stratospheric source of ozone in the tropical troposphere, *J. Atmos. Solar-Terr. Phys.* Vol. 60 , No. 1 , p. 27-36, 1998.
- Baray, J.-L., Leveau, J., Porteneuve, J., Ancellet, G., Keckhut, P., Posny, F., and Baldy, S.: Description and evaluation of a tropospheric ozone lidar implemented on existing lidar in the southern tropics, *App. Opt.*, Vol. 38, No. 33, 1999.
- Baray, J. L., Leveau, J., Baldy, S., Jouzel, J., Keckhut, P., Bergametti, G., Ancellet, G., Bencherif, H., Cadet, B., Carleer, M., David, C., De Mazière, M., Faduillhe, D., Godin-Beekmann, S., Goloub, P., Goutail, F., Metzger, J. M., Morel, B., Pommereau, J.P., Porteneuve, J., Portafaix, T., Posny, F., Robert, L., and Van Roozendael, M.: An instrumented station for the survey of ozone and climate change in the southern tropics: Scientific motivation, technical description and future plans, *J. Environm. Monit.*, 8, 1020-1028, doi:10.1039/b607762e, 2006.
- Baray, J.-L., Courcoux, Y., Keckhut, P., Portafaix, T., Tulet, P., Cammas, J.-P., Hauchecorne, A., Godin Beekmann, S., De Mazière, M., Hermans, C., Desmet, F., Sellegri, K., Colomb, A., Ramonet, M., Sciare, J., Vuillemin, C., Hoareau, C., Dionisi, D., Dufflot, V., Vèrèmes, H., Porteneuve, J., Gabarrot, F., Gaudo, T., Metzger, J.-M., Payen, G., Leclair de Bellevue, J., Barthe, C., Posny, F., Ricaud, P., Abchiche, A., and Delmas, R.: Maïdo Observatory: a new high-altitude station facility at Reunion Island (21°S, 55°E) for long-term atmospheric remote sensing and in situ measurements, *Atmos. Meas. Tech.*, 6, 2865-2877, doi:10.5194/amt-6-2865-2013, 2013.
- Bass, A.M. and Paur, R.J.: The ultraviolet cross-sections of ozone: I: The measurements, II: Results and temperature dependence, *Ozone Symposium, Greece*, 1984.
- Bègue, N., Vignelles, D., Berthet, G., Portafaix, T., Payen, G., Jégou, F., Benchérif, H., Jumelet, J., Vernier, J.-P., Lurton, T., Renard, J.-B., Clarisse, L., Duverger, V., Posny, F., Metzger, J.-M., and Godin-Beekmann, S.: Long-range isentropic transport of stratospheric aerosols over Southern Hemisphere following the Calbuco eruption in April 2015, *Atmos. Chem. Phys. Discuss.*, <https://doi.org/10.5194/acp-2017-544>, in review, 2017.
- Boynard, A., Hurtmans, D., Koukouli, M. E., Goutail, F., Bureau, J., Safieddine, S., Lerot, C. , Hadji-Lazaro, J. , Wespes, C., Pommereau, J.-P., Pazmino, A., Zyrichidou, I., Balis, D., Barbe, A., Mikhailenko, S. N., Loyola, D., Valks, P., Van Roozendael, M., Coheur, P.-F., and Clerbaux, C.: Seven years of IASI ozone retrievals from FORLI: validation with independent total column and vertical profile measurements, *Atmos. Meas. Tech.*, 9, 4327-4353, 2016.
- Clain, G., J. L. Baray, R. Delmas, R. Diab, J. Leclair de Bellevue, P. Keckhut, F. Posny, J. M. Metzger, and J. P. Cammas, Tropospheric O<sub>3</sub> climatology at two Southern Hemisphere tropical/subtropical sites, (Reunion Island and Irene, South Africa) from ozonesondes, LIDAR, and in situ aircraft measurements, *Atmos. Chem. Phys.*, 9, 1723-1734, 2009.
- Clain, G., Baray, J.-L., Delmas, R., Keckhut, P., and Cammas, J.-P.: A Lagrangian approach to analyse the tropospheric ozone climatology in the tropics: Climatology of stratosphere-troposphere exchange at Reunion Island, *Atmos. Environ.*, 44, 968-975, 2010.
- Clerbaux, C., Boynard, A., Clarisse, L., George, M., Hadji-Lazaro, J., Herbin, H., Hurtmans, D., Pommier, M., Razavi, A., Turquety, S., Wespes, C., and Coheur, P.-F.: Monitoring of atmospheric composition using the thermal infrared IASI/MetOp sounder, *Atmos. Chem. Phys.*, 9, 6041-6054, doi:10.5194/acp-9-6041-2009, 2009.

- Dionisi, D., Keckhut, P., Courcoux, Y., Hauchecorne, A., Porteneuve, J., Baray, J.-L., Leclair-de-Bellevue, J., Vèrèmes, H., Gabarrot, F., Decoupes, R., and Cammas, J.-P.: Water vapor observations up to the lower stratosphere through the Raman lidar during the Maïdo Lidar Calibration Campaign, *Atmos. Meas. Tech.*, 8, 1425-1445, 2015.
- Duflot, V., Dils, B., Baray, J.-L., De Mazière, M., Attié, J.-L., Vanhaelewyn, G., Senten, C., Vigouroux, C., Clain, G., and Delmas, R.: Analysis of the origin of the distribution of CO in the subtropical southern Indian Ocean in 2007, *J. Geophys. Res.*, 115, D22106, doi:10.1029/2010JD013994, 2010.
- Duflot et al., Reunion Island NDACC Lidars Operations 2013-2016 and the MORGANE campaign, NDACC Lidar Working Group, Payerne, Switzerland, 2016a.
- Duflot et al., Lidar UT/LS Observations at Reunion Island, WMO/SPARC/NDACC/GAW UT/LS Observations Workshop, Geneva, Switzerland, 2016b.
- Edwards, D. P., et al., Satellite-observed pollution from Southern Hemisphere biomass burning, *J. Geophys. Res.*, 111, D14312, doi:10.1029/2005JD006655, 2006.
- Gaudel, A., Ancellet, G., and Godin-Beekmann, S.: Analysis of 20 years of tropospheric ozone vertical profiles by lidar and ECC at Observatoire de Haute Provence (OHP) at 44°N, 6.7°E, *Atmospheric Environment*, doi:10.1016/j.atmosenv.2015.04.028, 2015.
- Godin S. et al, Ozone differential absorption lidar algorithm intercomparison, *Appl. Opt.*, 38, 6225-6236, 1999.
- Harris N., R.D. Hudson, and C. Phillips, Editors, WMO, SPARC/IOC Ozone Profile Trend Assessment, WMO Global Ozone Research and Monitoring Project - Report 43, Geneva, 1998.
- Hase, F., Blumenstock, T., and Paton-Walsh, C.: Analysis of the instrumental line shape of high-resolution Fourier transform IR spectrometers with gas cell measurements and new retrieval software, *Appl. Opt.*, 38, 3417-3422, 1999.
- Hinkley, E. D.: Laser monitoring of the atmosphere, *Topics in applied physics*, 14, Springer-Verlag, New York, 380 pp., 1976.
- Hoareau, C., Keckhut, P., Baray, J.-L., Robert, L., Courcoux, Y., Porteneuve, J., Vömel, H., and Morel, B.: A Raman lidar at La Reunion (20.8°S, 55.5°E) for monitoring water vapour and cirrus distributions in the subtropical upper troposphere: preliminary analyses and description of a future system, *Atmos. Meas. Tech.*, vol. 5, no. 6, pp. 1333-1348, 2012.
- Hurtmans, D., Coheur, P.-F., Wespes, C., Clarisse, L., Scharf, O., Clerbaux, C., Hadji-Lazaro, J., George, M., and Turquety, S.: FORLI radiative transfer and retrieval code for IASI, *J. Quant. Spectrosc. Ra.*, 113, 1391-1408, doi:10.1016/j.jqsrt.2012.02.036, 2012.
- Johnson, B. J., S. J. Oltmans, H. Vömel, H. G. J. Smit, T. Deshler, and C. Kroeger, ECC Ozone sonde pump efficiency measurements and tests on the sensitivity to ozone of buffered and unbuffered ECC sensor cathode solutions, *J. Geophys. Res.*, 107(D19), 4393, doi:10.1029/2001JD000557, 2002.
- Johnson, B. J. et al., Sensor solutions for the ECC ozonesondes, WMO-GAW-SHADOZ-NDACC Ozone Sonde Experts Workshop, Edinburgh, Scotland, 2016.
- Keckhut et al., Review of ozone and temperature lidar validations performed within the framework of the Network for the Detection of Stratospheric Change, *J. Environ. Monit.*, 2004.
- Keckhut, P., Courcoux, Y., Baray, J.-L., Porteneuve, J., Vèrèmes, H., Hauchecorne, A., Dionisi, D., Posny, F., Cammas, J.-P., Payen, G., Gabarrot, F., Evan, S., Khaykin, S., Rüfenacht, R., Tschanz, B., Kämpfer, N., Ricaud, P., Abchiche, A., Leclair-de-Bellevue, J., and Duflot, V.: Introduction to the Maïdo Lidar Calibration Campaign dedicated to the validation of upper air meteorological parameters, *J. Appl. Remote Sens.*, vol. 9, no. 1, 094099-094099, 2015.
- Khaykin S., A. Hauchecorne, J. Porteneuve, J.-F. Mariscal, E. D'Almeida, J.-P. Cammas, G. Payen, S. Evan, P. Keckhut, Ground-based Rayleigh-Mie Doppler lidar for wind measurements in the middle atmospheres, *ILRC 27*, 10.1051/epjconf/201611913005, 2016.

- Komhyr, W. D., Barnes, R. A., Brothers, G. B., Lathrop, J. A., and Opperman, D. P: Electrochemical concentration cell ozonesonde performance evaluation during STOIC 1989, *J. Geophys. Res.*, 100, 9231-9244, 1995.
- Kovalev V. A., Eichinger W. E., *Elastic Lidar: Theory, Practice, and Analysis Methods*, Wiley Edition, ISBN: 978-0-471-20171-7, 2004.
- Lacis, A. A., Wuebbles, D. J., and Logan, J. A.: Radiative Forcing of Climate by Changes in the Vertical Distribution of Ozone, *J. Geophys. Res.*, 95(D7), 9971-9981, 1990.
- 5 Leblanc et al.: Proposed standardized definitions for vertical resolution and uncertainty in the NDACC lidar ozone and temperature algorithms - Part 1: Vertical resolution, *Atmos. Meas. Tech.*, 9, 4029-4049, doi:10.5194/amt-9-4029-2016, 2016a.
- Leblanc et al.: Proposed standardized definitions for vertical resolution and uncertainty in the NDACC lidar ozone and temperature algorithms - Part 2: Ozone DIAL uncertainty budget, *Atmos. Meas. Tech.*, 9, 4051-4078, doi:10.5194/amt-9-4051-2016, 2016b.
- 10 Leclair De Bellevue J., Réchou A., Baray J.-L., Ancellet G., and Diab R. D., Signatures of stratosphere to troposphere transport near deep convective events in the southern subtropics, *J. Geophys. Res.*, VOL. 111, D24107, doi:10.1029/2005JD006947, 2006
- Martin, R. V., Jacob, D. J. , Yantosca, R. M., Chin, M., and Ginoux, P.: Global and regional decreases in tropospheric oxidants from photochemical effects of aerosols, *J. Geophys. Res.*, 108(D3), 4097, doi:10.1029/2002JD002622, 2003.
- McGee, T. J., Gross, M., Ferrare, R., Heaps, W., and Singh, U.: Raman dial measurements of stratospheric ozone in the presence of volcanic aerosols, *Geophys. Res. Lett.*, 20, 955-958, doi:10.1029/93GL00751, 1993.
- 15 Molina L. T. and Molina M. J., Absolute absorption cross sections of ozone in the 185 to 350nm wavelength range, *J. Geophys. Res.* 91, 14, 501-14, 508, 1986.
- Morel et al., Evidence of tidal perturbations in the middle atmosphere over Southern Tropics as deduced from LIDAR data analyses, *J. of Atmos. and Solar-Terrestrial Phys.*, 2002.
- 20 Pelon J., *Distribution verticale de l'ozone dans la troposphère et la stratosphère: étude expérimentale par télédétection laser et application aux échanges troposphère-stratosphère*, Thèse de l'Université Paris 06, 1985.
- Portafaix et al., Fine-scale study of a thick stratospheric ozone lamina at the edge of the southern subtropical barrier, *J. Geophys. Res.*, 2003.
- Portafaix T., S. Godin-Beekmann, G. Payen, M. de Mazière, B. Langerock, S. Fernandez, F. Posny, J.P. Cammas, J. M. Metzger, H. Bencherif, C. Vigouroux and N. Marquestaut, Ozone profiles obtained by DIAL technique at Maïdo Observatory in La Reunion Island: comparisons with ECC ozone-sondes, ground-based FTIR spectrometer and microwave radiometer measurements, *ILRC 27*, 10.1051/epj-conf/201611905005, 2015.
- 25 Posny, F., Johnson, B. J., Metzger, J.-M., Duflot, V., Portafaix, T., Cullis, P., Thompson, A.M., Witte, J. C., La Reunion Island (21°S, 55.5°E) SHADOZ/NDACC station: First re-processed ozonesonde data and comparisons with lidar measurements at the Maïdo Observatory, *Quadriennal Ozone Symposium of the International Ozone Commission*, QOS2016-192, 2016.
- 30 Rodgers C., *Inverse Methods for Atmospheric Sounding: Theory and Practice*, Series on Atmospheric, Oceanic and Planetary Physics, vol. 2, World Sci., Singapore, 2000.
- Rodgers, C. D. and Connor, B. J.: Intercomparison of remote sounding instruments, *J. Geophys. Res.*, 108, 4116, doi:10.1029/2002JD002299, 2003.
- Savitzky A. and Golay M. J. E., Smoothing and Differentiation of Data by Simplified Least Squares Procedures, *Anal. Chem.*, 1964, 36 (8), pp 1627-1639, DOI: 10.1021/ac60214a047, Publication Date: July 1964
- 35 Sivakumar et al., Rayleigh LIDAR and satellite (HALOE, SABER, CHAMP and COSMIC) measurements of stratosphere-mesosphere temperature over a southern sub-tropical site, Reunion (20.8°S; 55.5°E): climatology and comparison study, *Ann. Geophys.*, 2011a.

- Sivakumar V., Bencherif H., Bègue N., Thompson A. N., Tropopause Characteristics and Variability from 11 yr of SHADOZ Observations in the Southern Tropics and Subtropics, *J. App. Met. Clim.*, 2011b.
- Smit et al., Assessment of the performance of ECC-ozonesondes under quasi-flight conditions in the environmental simulation chamber: Insights from the Juelich Ozone Sonde Intercomparison Experiment (JOSIE), *J. Geophys. Res.*, 2007.
- 5 Smit, H. G. J., and the Panel for the Assessment of Standard Operating Procedures for Ozonesondes (ASOPOS), Guidelines for homogenization of ozonesonde data, SI2N/O3S-DQA activity as part of "Past changes in the vertical distribution of ozone assessment", available at: [http://www-das.uwyo.edu/%7EEdeshler/NDACC\\_O3Sondes/O3s\\_DQA/O3S-DQA-Guidelines%20Homogenization-V2-19November2012.pdf](http://www-das.uwyo.edu/%7EEdeshler/NDACC_O3Sondes/O3s_DQA/O3S-DQA-Guidelines%20Homogenization-V2-19November2012.pdf), 2012.
- Smit et al., Ozone Data Quality Assessment (O3S-DQA): Resolving inhomogeneities in long-term ozone sounding records and assessing their uncertainties, Quadriennial Ozone Symposium of the International Ozone Commission, QOS2016-246, 2016.
- 10 Stevenson, D. S., Dentener, F. J., Schultz, M. G., Ellingsen, K., van Noije, T. P. C., Wild, O., Zeng, G., Amann, M., Atherton, C. S., Bell, N., Bergmann, D. J., Bey, I., Butler, T., Cofala, J., Collins, W. J., Derwent, R. G., Doherty, R. M., Drevet, J., Eskes, H. J., Fiore, A. M., Gauss, M., Hauglustaine, D. A., Horowitz, L. W., Isaksen, I. S. A., Krol, M. C., Lamarque, J.-F., Lawrence, M. G., Montanaro, V., Müller, J.-F., Pitari, G., Prather, M. J., Pyle, J. A., Rast, S., Rodriguez, J. M., Sanderson, M. G., Savage, N. H., Shindell, D. T., Strahan, S. E., Sudo,
- 15 K., and Szopa, S.: Multimodel ensemble simulations of presentday and near-future tropospheric ozone, *J. Geophys. Res.*, 111, D08301, doi:10.1029/2005JD006338, 2006.
- Sullivan, J. T., McGee, T. J., DeYoung, R., Twigg, L. W., Sunnicht, G. K., Pliutau, D., Knepp, T., and Carrion, W.: Results from the NASA GSFC and LaRC Ozone Lidar Intercomparison: New Mobile Tools for Atmospheric Research, *Journal of Atmospheric and Oceanic Technology*, 10.1175/JTECH-D-14-00193.1, 2015.
- 20 Thompson, A. M., Balashov, N. V., Witte, J. C., Coetzee, J. G. R., Thouret, V., and Posny, F.: Tropospheric ozone increases over the southern Africa region: bellwether for rapid growth in Southern Hemisphere pollution?, *Atmos. Chem. Phys.*, 14, 9855-9869, 2014.
- Uchino O., T. Sakai, T. Nagai, I. Morino, T. Maki, M. Deushi, K. Shibata, M. Kajino, T. Kawasaki, T. Akaho, S. Takubo, H. Okumura, K. Arai, M. Nakazato, T. Matsunaga, T. Yokota, S. Kawakami, K. Kita, and Y. Sasano, DIAL measurement of lower tropospheric ozone over Saga (33.24°N, 130.29°E), Japan, and comparison with a chemistry-climate model, *Atmos. Meas. Tech.*, 7, 1385-1394, 2014.
- 25 Vèrèmes et al., Multiple subtropical stratospheric intrusions over Reunion Island: observational, eulerian and lagrangian numerical modeling approaches, *J. Geophys. Res.*, doi: 10.1002/2016JD025330, 2016.
- Vèrèmes H., G. Payen, P. Keckhut, V. Duflet, J.-L. Baray, J.-P. Cammas, J. Leclair de Bellevue, S. Evan, F. Posny, F. Gabarrot, J.-M. Metzger, N. Marquestaut, S. Meier, H. Vömel, and R. Dirksen, A Raman lidar at Maïdo Observatory (Reunion Island) to measure water vapor in the troposphere and lower stratosphere: calibration and validation, *Atmos. Meas. Tech. Discuss.*, doi:10.5194/amt-2017-32, 2017.
- 30 Vigouroux, C., De Mazière, M., Demoulin, P., Servais, C., Hase, F., Blumenstock, T., Kramer, I., Schneider, M., Mellqvist, J., Strandberg, A., Velasco, V., Notholt, J., Sussmann, R., Stremme, W., Rockmann, A., Gardiner, T., Coleman, M., and Woods, P.: Evaluation of tropospheric and stratospheric ozone trends over Western Europe from ground-based FTIR network observations, *Atmos. Chem. Phys.*, 8, 6865-6886, 2008.
- Witte Jacquelyn C., Anne M. Thompson, Herman G. J. Smit, Masatomo Fujiwara, Françoise Posny, Gert J. R. Coetzee, Edward T. Northam, Bryan J. Johnson, Chance W. Sterling, Maznorizan Mohammed, Shin-Ya Ogino, Allen Jordan, Zamuna Zainel, and Francisco R. da Silva, First reprocessing of Southern Hemisphere ADditional OZonesondes (SHADOZ) profile records (1998-2015) 1: Methodology and evaluation, *J. Geophys. Res.*, in review.



Zhou, M., Vigouroux, C., Langerock, B., Wang, P., Dutton, G., Hermans, C., Kumps, N., Metzger, J.-M., Toon, G., and De Mazière, M.: CFC-11, CFC-12 and HCFC-22 ground-based remote sensing FTIR measurements at Reunion Island and comparisons with MIPAS/ENVISAT data, *Atmos. Meas. Tech. Discuss.*, doi:10.5194/amt-2016-235, in review for *Atmos. Meas. Tech.*, 2016.

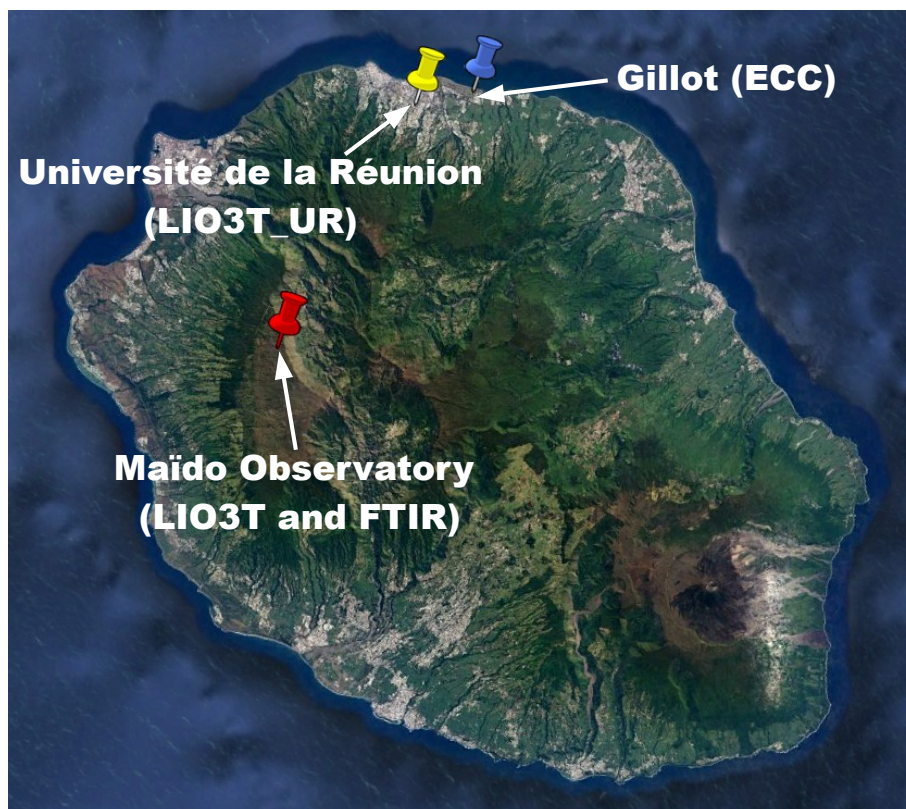


**Figure 1.** Map showing the locations of the different measurement sites (Maïdo Observatory, Gillot, and University in Reunion Island) and instruments ( $\text{LIO3T}_{UR}$ , ECC, FTIR and LIO3T) used in this study.

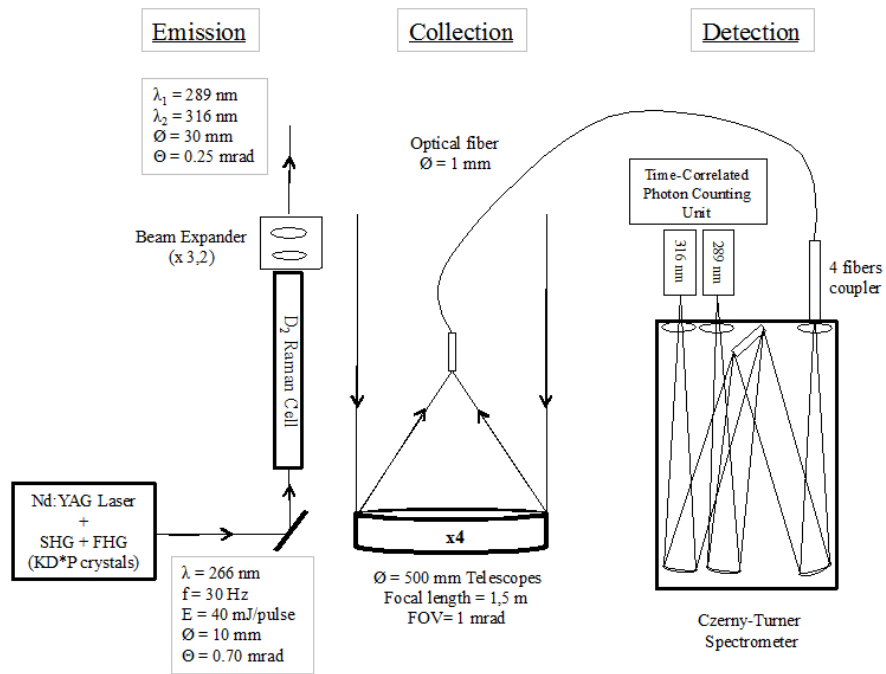


**Figure 2.** LIO3T instrumental schema.

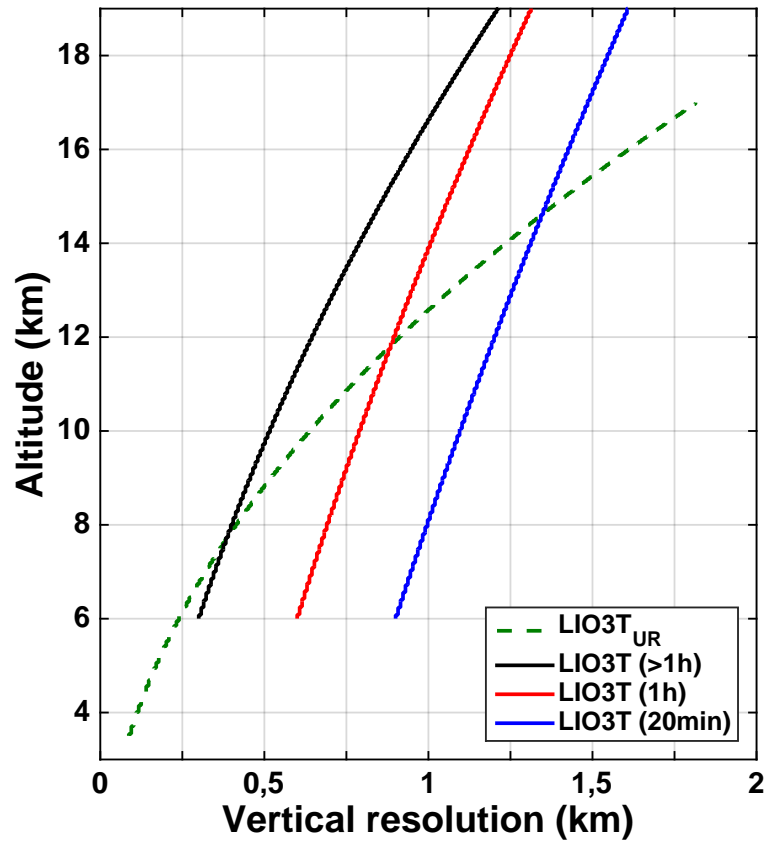


**Figure 3.** Mean vertical resolution of LIO3T<sub>UR</sub> profiles (dashed green curve) and of LIO3T profiles for integration times greater than 1 hour (black curve), equal to 1 hour (red curve) and equal to 20 minutes (blue curve).

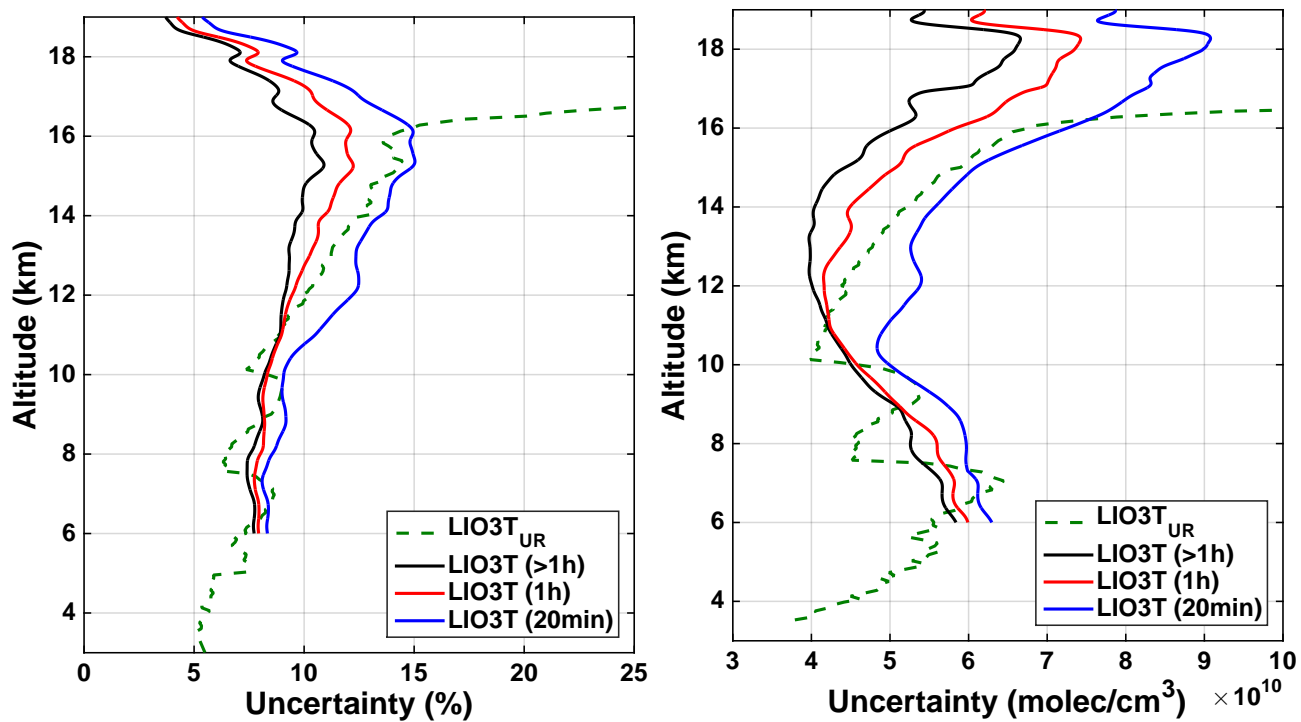


**Figure 4.** Mean uncertainties in % (left panel) and molec/cm<sup>3</sup> (right panel) of the LIO3T<sub>UR</sub> profiles (dashed green curve) and of the LIO3T profiles for integration times greater than 1 hour (black curve), equal to 1 hour (red curve) and equal to 20 minutes (blue curve).

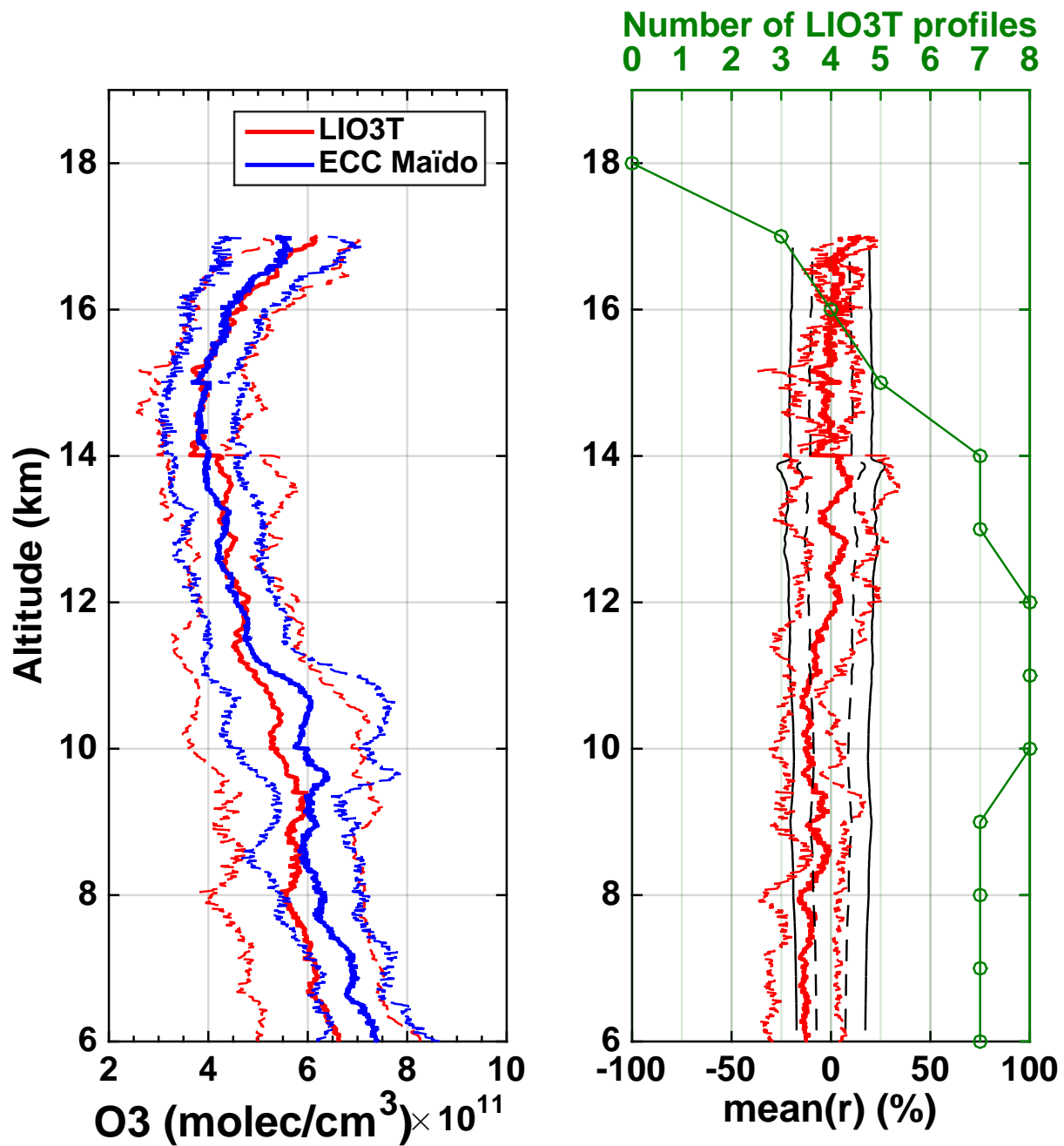


**Figure 5.** Left panel: mean LIO3T O<sub>3</sub> profile (red curve) and mean ECC profile (blue curve) measured during the 8 intercomparison measurements performed at Maïdo. The dashed lines give the 1 standard deviation around the mean; Right panel: mean *r* between the LIO3T and ECC profiles (red curve), mean LIO3T uncertainty around zero (black dashed lines) and mean LIO3T uncertainty + ECC precision around zero (black lines). The red dashed lines give the 1 standard deviation around the *r* mean. The green line (upper X-axis) gives the number of LIO3T profiles used for comparison.

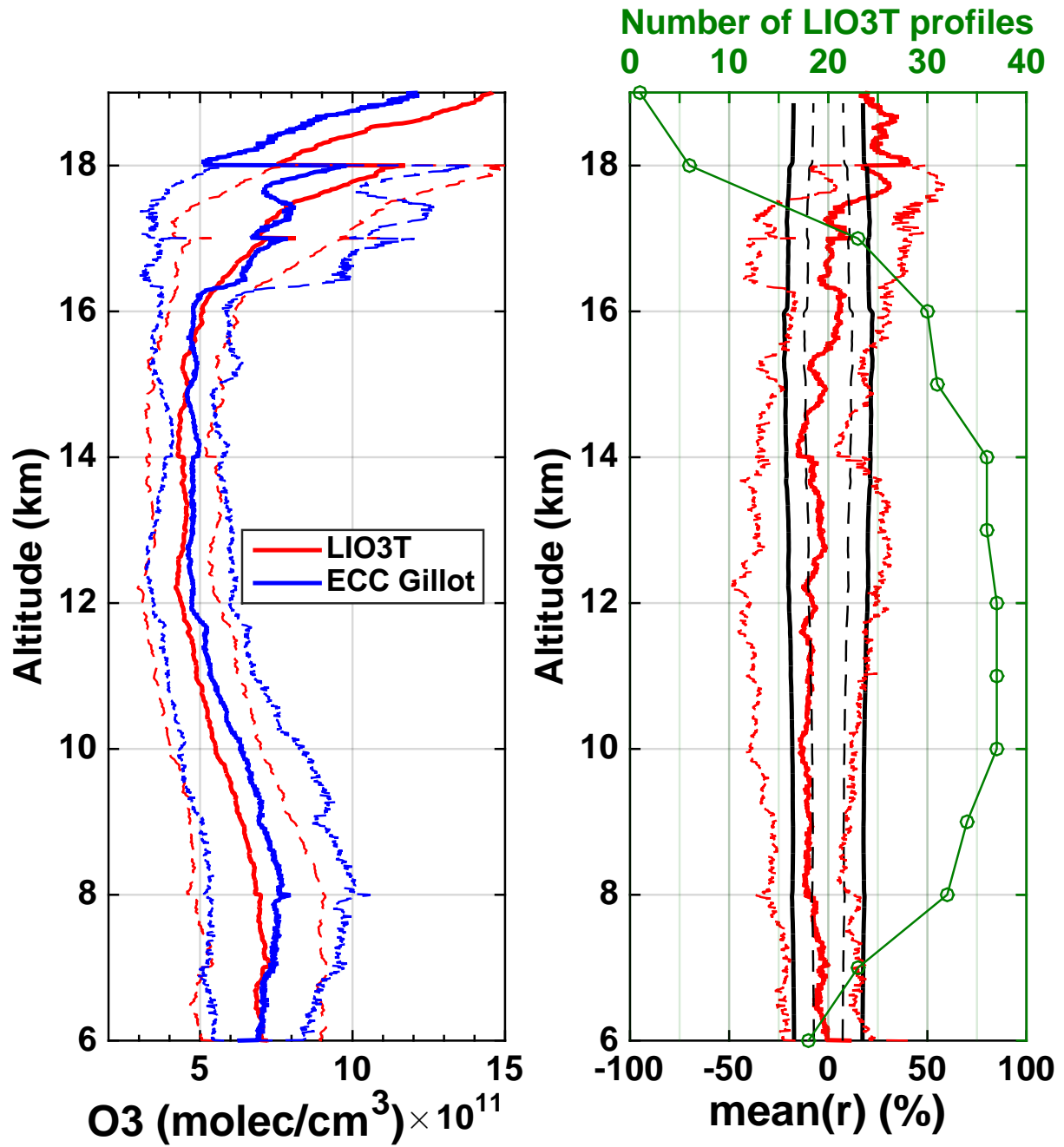
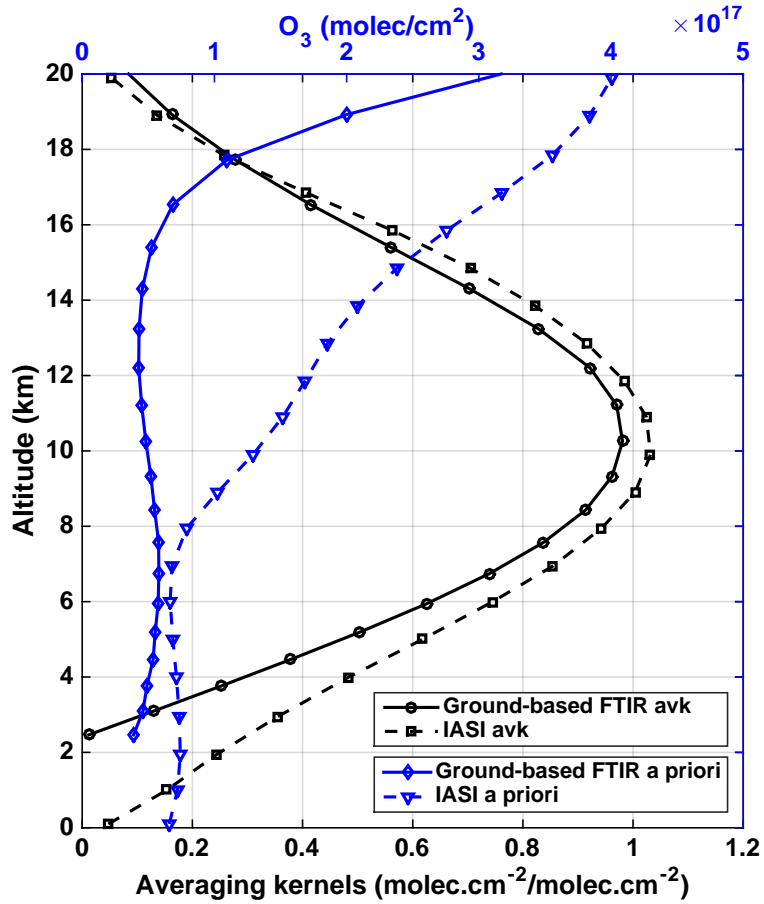
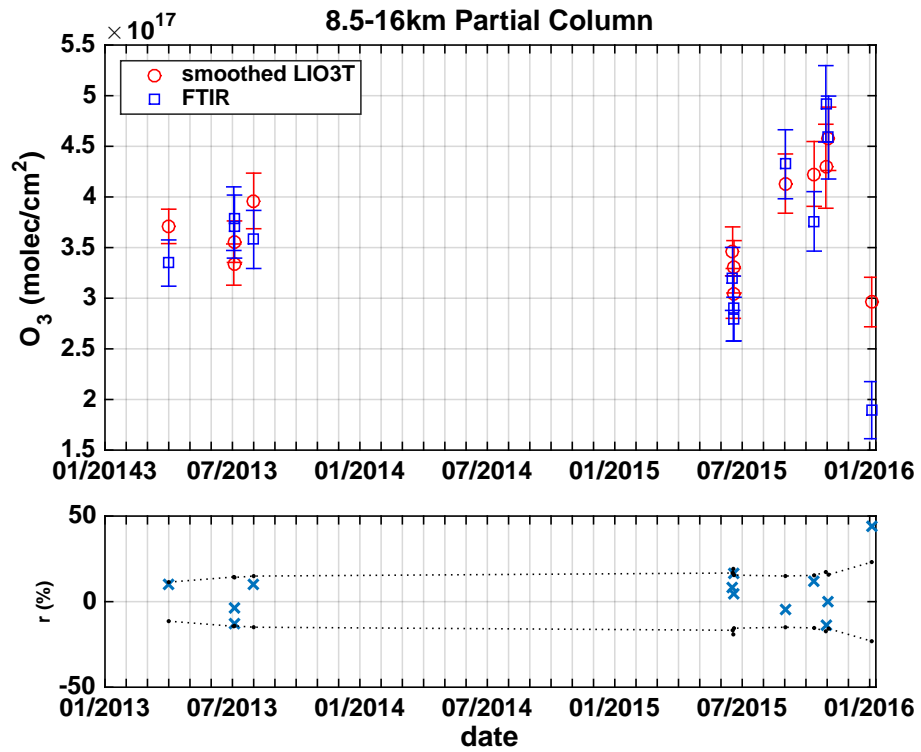


Figure 6. Same as Figure 5 for NDACC/SHADOZ Gillot ECC soundings and "full night" LIO3T profiles.



**Figure 7.** Lower X-axis: ground-based NDACC FTIR (black curve and circles) and IASI (black dashed curve and squares) averaging kernels for the 8-16 km and 6-16km partial columns, respectively; Upper X-axis: ground-based NDACC FTIR (blue curve and diamonds) and IASI (blue dashed curve and triangles) O<sub>3</sub> a priori profiles.





**Figure 8.** Upper panel: smoothed LIO3T (red circles) and ground-based NDACC FTIR (blue squares) 8.5-16km O<sub>3</sub> partial columns. Vertical bars give uncertainties for each measurement; Lower panel:  $r$  (%) between LIO3T and FTIR measurements (blue crosses) superimposed on LIO3T + FTIR uncertainties around zero (black dotted lines and dots).

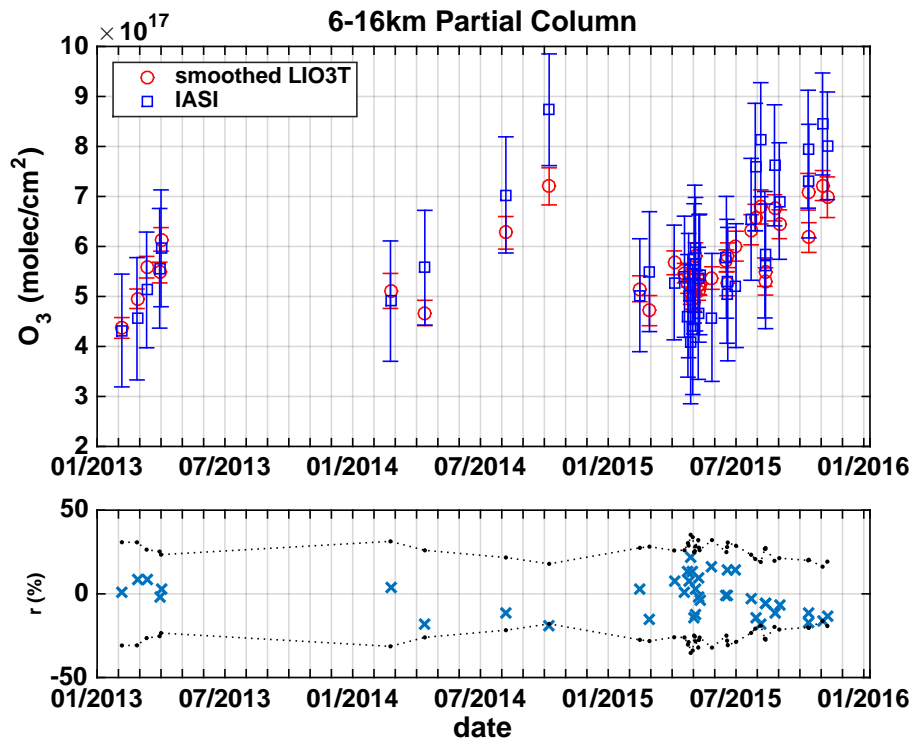


**Figure 9.** Upper panel: smoothed LIO3T (red circles) and IASI (blue squares) 6-16km  $O_3$  partial columns. Vertical bars give uncertainties for each measurement; Lower panel:  $r$  (%) between LIO3T and IASI measurements (blue crosses) superimposed on LIO3T + IASI uncertainties around zero (black dotted lines and dots).

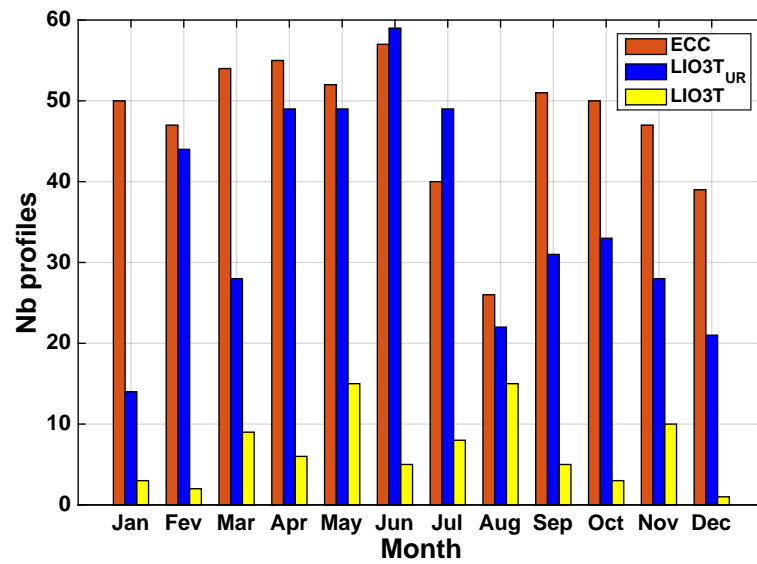


**Figure 10.** Number of O<sub>3</sub> profiles per month for ECC (1998-2015, 568 profiles), LIO3T<sub>UR</sub> (1998-2010, 427 profiles) and LIO3T (January 2013-January 2016, 84 profiles).

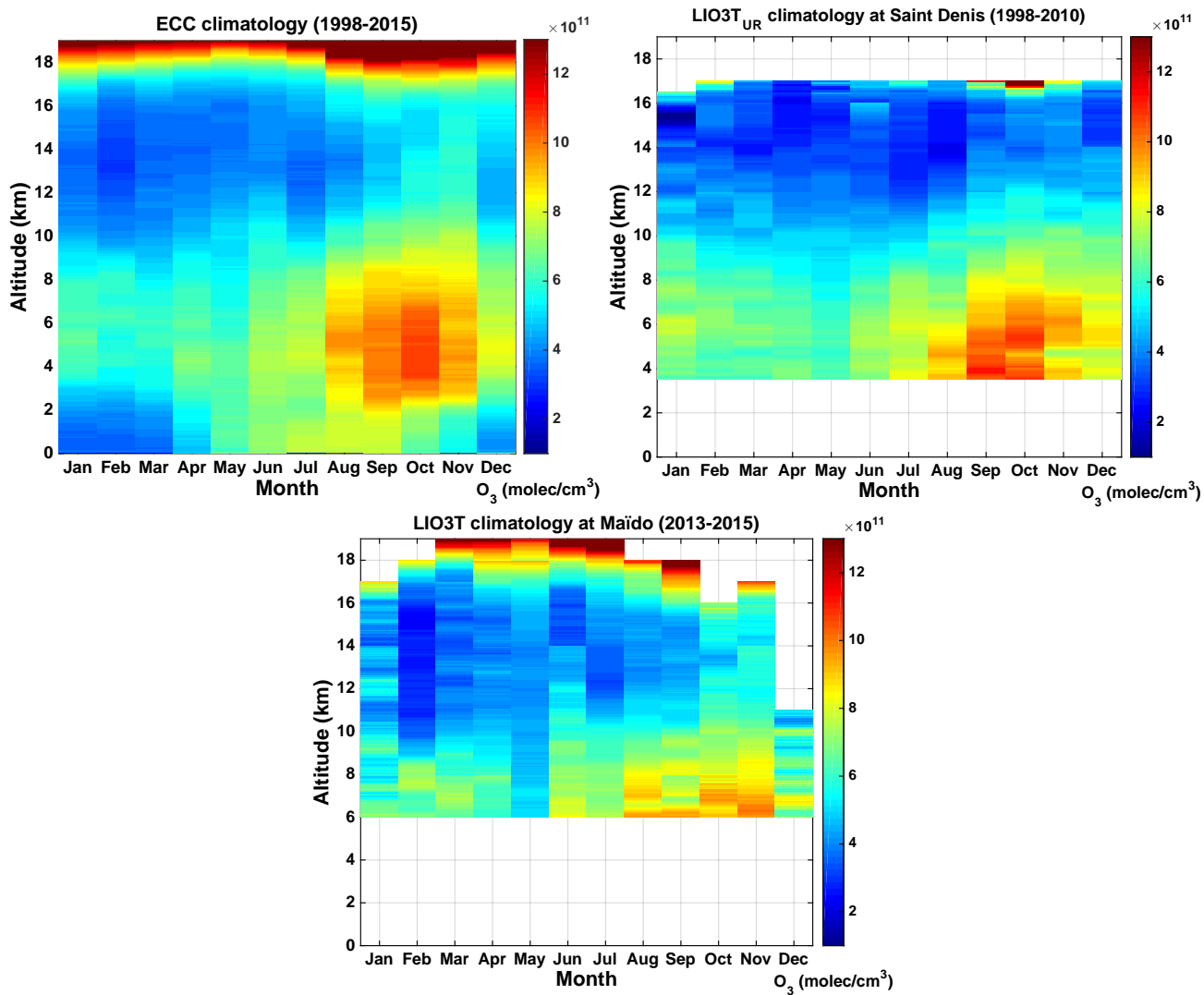


**Figure 11.** Monthly  $O_3$  climatology between 0 and 19km derived from ECC sondes over 1998-2015 at Gillot site (Top left panel), from LIO3T<sub>UR</sub> over 1998-2010 at Université de la Réunion campus site (Top right panel) and from LIO3T over 2013-2015 at Maïdo Observatory (including data routinely performed and from intensive period of observations) (bottom panel).

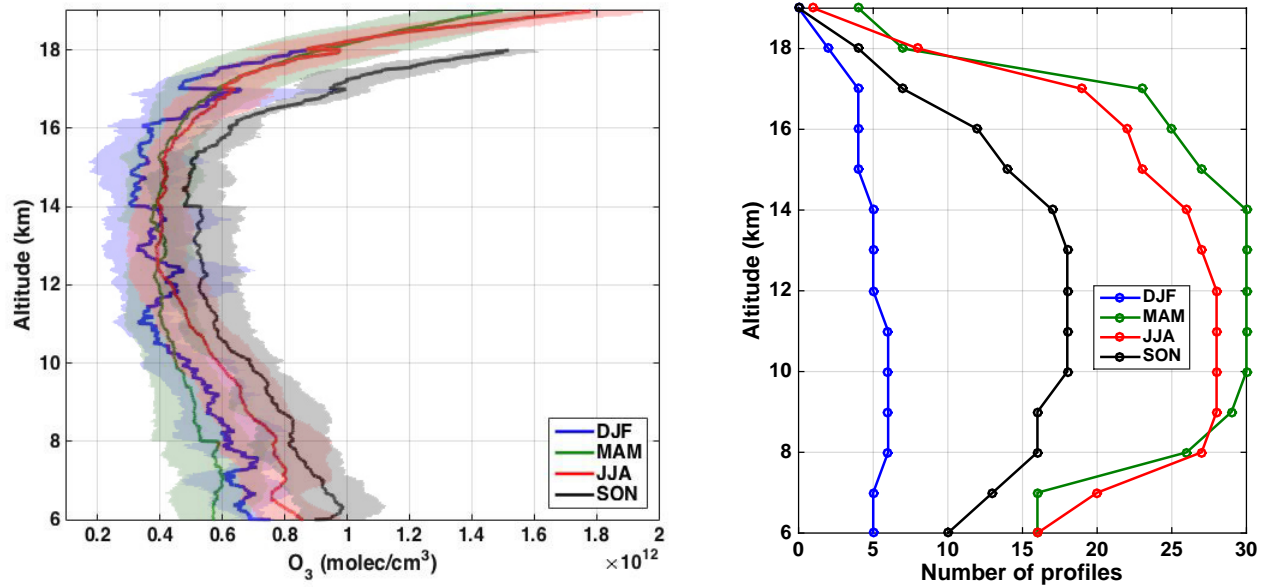


**Figure 12.** Left panel: Seasonal LIO3T O<sub>3</sub> profiles for DJF (blue curve - 8 profiles), MAM (green curve - 30 profiles), JJA (red curve - 25 profiles) and SON (black curve - 21 profiles). The shaded areas give the 1 standard deviation around the mean. Right panel: Number of LIO3T profiles used for each climatological profile.

<b>Site</b>	<b>Latitude</b>	<b>Longitude</b>	<b>Altitude (m)</b>	<b>Distance to Maïdo (km)</b>
Gillot	20.893°S	55.529 °E	9	26
University	20.902°S	55.485 °E	80	23
Maïdo Observatory	21.079 °S	55.383 °E	2160	0

**Table 1.** Coordinates and distance to Maïdo Observatory of the observation sites used in this study.

<b>Date</b>	<b>Profile valid range (km)</b>
2013/06/24	6-14
2013/06/25	6-14
<i>2015/05/11</i>	6-17
<i>2015/05/15</i>	10-16
<i>2015/05/26</i>	6-12
<i>2015/05/28</i>	6-17
<i>2015/07/06</i>	6-15
<i>2015/07/07</i>	6-17

**Table 2.** Dates of comparisons with collocated ECC soundings and corresponding LIO3T O<sub>3</sub> profile valid ranges. Italicized dates indicate profiles impacted by the Calbuco eruption.